J. Fluid Mech. (2014), *vol.* 757, *pp.* 573–598.
doi:10.1017/jfm.2014.474

Unconfined turbulent entrainment across density interfaces

Ajay B. Shrinivas[1] **and Gary R. Hunt**[2,†]

[1]Department of Civil and Environmental Engineering, Imperial College London, London SW7 2AZ, UK

[2]Department of Engineering, University of Cambridge, Trumpington Street, Cambridge CB2 1PZ, UK

(Received 27 March 2014; revised 16 June 2014; accepted 11 August 2014;
first published online 23 September 2014)

We present theoretical models describing the quasi-steady downward transport of buoyant fluid across a gravitationally stable density interface separating two unbounded quiescent fluid masses. The primary transport mechanism is turbulent entrainment resulting from the localised impingement of a vertically forced high-Reynolds-number axisymmetric jet with steady source conditions. The entrainment across the interface is examined in the large-time asymptotic state, wherein the interfacial gravity current, formed by the fluid entrained from the upper layer and the jet, becomes infinitesimally thin and a two-layer stratification persists. Characterising flows with small interfacial Froude numbers (Fr_i) as an axisymmetric semi-ellipsoidal impingement dome, we combine conservation equations with a mechanistic model of entrainment and reveal that, in this regime, the dimensionless entrainment flux E_i across the interface follows the power law $E_i = 0.24\mathrm{Fr}_i^2$. For large-$\mathrm{Fr}_i$ impingements, modelled as a fully penetrating turbulent fountain, we show that E_i no longer scales with Fr_i^2, but linearly on Fr_i, following $E_i = 0.42\mathrm{Fr}_i$. We establish the intermediate range of Fr_i over which there is a transition between these quadratic and linear power laws, thus enabling us to classify the dynamics of entrainment across the interface into three distinct regimes. Finally, the close agreement of our solutions with existing experimental results is illustrated.

Key words: geophysical and geological flows, plumes/thermals, stratified flows

1. Introduction

The excitation by turbulent motions of a gravitationally stable horizontal interface separating two uniform fluid masses of different density gives rise to the entrainment of buoyant fluid across the interface. This classic transport phenomenon, characterised by the interaction between a stable density stratification and the destabilising effects of interfacial turbulence, plays a key role in a wide range of geophysical and engineering flows. Turbulent entrainment at the boundary between the lowest layer of the Earth's atmosphere and the stratosphere is instrumental in determining global weather patterns. Furthermore, the resulting vertical exchange of atmospheric chemicals can contribute to the depletion of the ozone layer and to the formation of acid precipitation (Shapiro 1980). Wind-induced shear stresses on the surface of a stratified ocean give rise to turbulent motions in the upper regions that drive the entrainment of underlying denser

† Email address for correspondence: gary.hunt@eng.cam.ac.uk

water across the thermocline, a thin transitional layer. Seasonal variations of the thermocline influence marine ecosystems, ocean circulation and sonar performance (Zhang *et al.* 2012). In low-energy building ventilation, jets of cool air injected upwards by mechanical underfloor diffusers (Lin & Linden 2005), or that form naturally as air flows in via low-level openings (Hunt & Coffey 2010), may impinge on thermal interfaces separating warm and cooler regions of a room. The resulting entrainment fluxes across the interface(s) governs the internal temperatures and ventilation efficiency, thereby directly influencing the comfort of occupants.

Fuelled by the aim of determining the rate of entrainment across an interface, a significant number of studies have stemmed from the pioneering work of Rouse & Dodu (1955). By considering the vertical oscillation of a rectangular grid positioned parallel to, and some distance below, a horizontal density interface, Rouse & Dodu (1955) examined the deepening of a turbulent lower layer due to the entrainment of relatively light fluid from an overlying quiescent layer. Turner (1968) postulated that the lower layer deepens at a rate controlled primarily by the interaction between the local turbulent motions and the interface. Accordingly, he hypothesised that the entrainment rate be parameterised purely in terms of quantities local to the interface, namely, the characteristic length scale of the impinging eddies, the turbulence intensity and the interfacial buoyancy jump. Turner's hypothesis has since formed the cornerstone of the research on entrainment across interfaces.

Baines (1975) considered an axisymmetric turbulent plume incident with an interface separating two initially homogeneous layers of different density. In accordance with Turner's hypothesis, Baines deduced that the volume flux Q_e turbulently entrained across the interface is dependent on the local plume radius b_i, vertical plume velocity w_i (the subscript 'i' reading 'at the interface') and the buoyancy difference $\Delta g'$ across the interface. Forming an interfacial Froude number $\mathrm{Fr}_i = w_i/\sqrt{b_i \Delta g'}$, which characterises the relative strengths of the destabilising inertial forcing and the stabilising buoyancy force, Baines (1975) showed that the dimensionless entrainment flux $E_i = Q_e/(\pi b_i^2 w_i)$ follows the power law

$$E_i = A\mathrm{Fr}_i^n, \tag{1.1}$$

with $n = 3$ and $A = 0.07$ (figure 1). Whilst this form of entrainment law (1.1) has not been in dispute, there is currently an unresolved debate over the value of the exponent n.

Investigating the interaction of discrete vortex rings with a sharp density interface, Linden (1973) showed that his experimental results, and a theoretical model of the vortex–interface interaction, support an $E_i \propto \mathrm{Fr}_i^3$ entrainment law. Kumagai (1984) considered the same experimental configuration as Baines (1975) and based on measurements of the entrainment rate (figure 1), he proposed the empirical relationship

$$E_i = \frac{\mathrm{Fr}_i^3}{1 + 3.1\mathrm{Fr}_i^2 + 1.8\mathrm{Fr}_i^3}. \tag{1.2}$$

From (1.2), $E_i \propto \mathrm{Fr}_i^3$ for $\mathrm{Fr}_i \ll 1$ and $E_i \to 0.56$ for $\mathrm{Fr}_i \gg 1$. Interestingly, Kumagai argues that Linden's data in fact suggests a power-law exponent of $n \approx 2$ for small Fr_i, rather than $n = 3$. More recently, Coffey & Hunt (2010) examined, within the confines of a box, the interfacial mixing induced by the impingement of a turbulent inflowing fresh water jet (via an opening at the top) on a dense saline layer draining from the box (via an opening at the base). Their measurements also suggested $E_i \propto \mathrm{Fr}_i^3$ for $\mathrm{Fr}_i < 1$ and that E_i tends to a constant value for $\mathrm{Fr}_i > 1$.

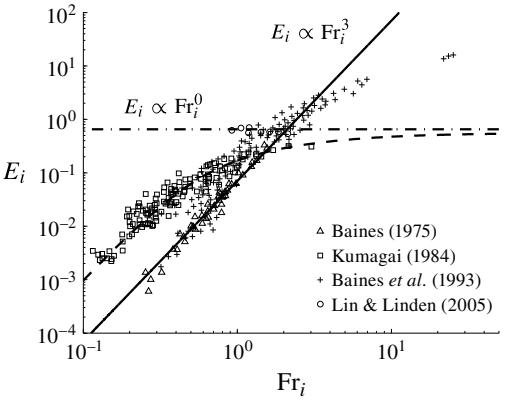

FIGURE 1. Experimental measurements of the dimensionless entrainment flux E_i against the interfacial Froude number Fr_i. The solid line ($E_i = 0.07\mathrm{Fr}_i^3$), dashed line (1.2) and dashed-dotted line ($E_i = 0.65$) are the empirical relationships of Baines (1975), Kumagai (1984) and Lin & Linden (2005), respectively.

Cardoso & Woods (1993) examined the volume flux turbulently entrained by the top of a rising axisymmetric plume from a stratified upper layer across an interface into an almost uniform lower layer. Building on the energy arguments of Linden (1975), their model assumes that a constant fraction of the kinetic energy supplied at the interface by the plume, energy for turbulent entrainment, is converted into the potential energy of the stratification. This elegant energetic formulation yields $E_i \propto \mathrm{Fr}_i^2$, consistent with their experimental results. Notably, they identified that an entrainment law of this quadratic form provides a better fit to Kumagai's (1984) data for $\mathrm{Fr}_i \lesssim 1$ than his $E_i \propto \mathrm{Fr}_i^3$. This $n = 2$ result is also in agreement with the experimental measurements, and complementary scaling arguments, of Ching, Fernando & Noh (1993) who investigated the impingement of a turbulent line plume on a sharp density interface.

Baines, Corriveau & Reedman (1993) considered a turbulent fountain formed by the vertical upward injection of dense fluid from the base of a box into a relatively light environment. Measurements of the entrainment flux into the fountain from above a deepening lower layer indicated that $E_i \propto \mathrm{Fr}_i^3$ for $\mathrm{Fr}_i \lesssim 1.5$. As the flow, pre-impingement, was negatively buoyant we have referred to this type of experiment (table 1) as 'impinging fountain'. They challenge Kumagai's (1984) constant-E_i result for $\mathrm{Fr}_i \gg 1$ and argue instead, that in this limit E_i should increase linearly with Fr_i (for $\mathrm{Fr}_i \gtrsim 1.5$) given that the momentum flux of the fountain driving the entrainment increases with Fr_i.

Several other contradictory entrainment laws have been proposed. Lin & Linden (2005) considered the impingement of a turbulent fountain on a steady interface and found that E_i was approximately constant at $E_i = 0.65$ for $0.9 \lesssim \mathrm{Fr}_i \lesssim 2.2$. The oscillating-grid experiments of McDougall (1978) and Fernando & Long (1983) support the (conflicting) results that $n = 2.2$ and $n = 3.5$, respectively; as these two studies give the entrainment rate in terms of an entrainment velocity, we inferred the entrained volume flux from the product of this velocity and the constant plan area of their visual tank so as to express their findings in the form of (1.1).

Evidently, in the pursuit of a universal relationship that describes the dependence of E_i on Fr_i, the studies have given rise to conflicting power laws associated with a wide variation in the value of the exponent n, as highlighted in table 1. Fernando

Researcher(s)	n	Range of Fr_i	Type of experiment
Lin & Linden (2005)	0	$0.9 < \mathrm{Fr}_i < 2.2$	Impinging fountain
Baines *et al.* (1993)	1	$1.2 < \mathrm{Fr}_i < 26$	Impinging fountain
Cardoso & Woods (1993)	2	$0.3 < \mathrm{Fr}_i < 1.3$	Impinging plume
McDougall (1978)	2.2	$0.4 < \mathrm{Fr}_i < 1.2$	Oscillating grid
Baines (1975), Kumagai (1984)	3	$0.1 < \mathrm{Fr}_i < 1.5$	Impinging plume
Fernando & Long (1983)	3.5	$0.1 < \mathrm{Fr}_i < 0.6$	Oscillating grid

TABLE 1. Examples of the reported values of the exponent n in the entrainment law $E_i \propto \mathrm{Fr}_i^n$. Depending on the type of experiment, E_i and Fr_i are defined using the velocity and length scales at the interface of the plume/fountain with top-hat profiles, or of the mean motions induced by an oscillating grid.

(1991) concludes in his review on turbulent mixing in stratified fluids that in this field of research, the entrainment law has arguably been the most controversial of all topics and despite more than half a century of research as of 1955, there is no general consensus on the exact form of (1.1). At the time of writing there is still no consensus. Figure 1 plots the experimental data of E_i as a function of Fr_i from Baines (1975), Kumagai (1984), Baines *et al.* (1993) and Lin & Linden (2005). The conflicting entrainment laws are not altogether surprising given the significant amount of scatter in the data, with the experimentally inferred values of E_i varying by up to an order of magnitude for a given Fr_i.

In this paper, we revisit the fundamental question: what is the law that governs the rate of turbulent entrainment across a density interface? When this problem is examined within the confines of a box or visual tank, as is necessary in laboratory experiments, there is an inherent complex time-dependent coupling between the entrainment flux and the development of the stratification; one exception being the steady experiments of Lin & Linden (2005). To overcome this complexity, we consider theoretically the large-time quasi-steady flow in an unconfined environment (hence, our reference to 'unconfined' entrainment) that is induced, and maintained, by the impingement of a turbulent jet on a sharp density interface separating two quiescent homogeneous fluid masses. With a view to providing the theoretical basis for an entrainment law, in § 2 we establish a framework to analyse turbulent entrainment across the interface resulting from the impingement of the jet. In § 3, a model of small-Fr_i entrainment is developed and an analytic power-law solution for E_i obtained. Analysing our predictions in § 4, we elucidate the fundamental physics underlying our small-Fr_i entrainment law. We then present, in § 5, a model of large-Fr_i entrainment. In § 6, we classify the entrainment dynamics into three distinct regimes, characterised by interfacial impingements that may be regarded as weakly, moderately and highly energetic. We show in § 7 that our entrainment law

$$E_i = \begin{cases} 0.24\mathrm{Fr}_i^2 & \text{for } \mathrm{Fr}_i < 1.4, \\ 0.42\mathrm{Fr}_i & \text{for } \mathrm{Fr}_i > 3.8, \end{cases} \tag{1.3}$$

is in very good agreement with the extensive data sets of Kumagai (1984) for $\mathrm{Fr}_i \lesssim 1$ and Baines *et al.* (1993) for $\mathrm{Fr}_i \gtrsim 1$. In § 8, we draw our conclusions and discuss extensions to our work, including interfacial entrainment within the confines of a box.

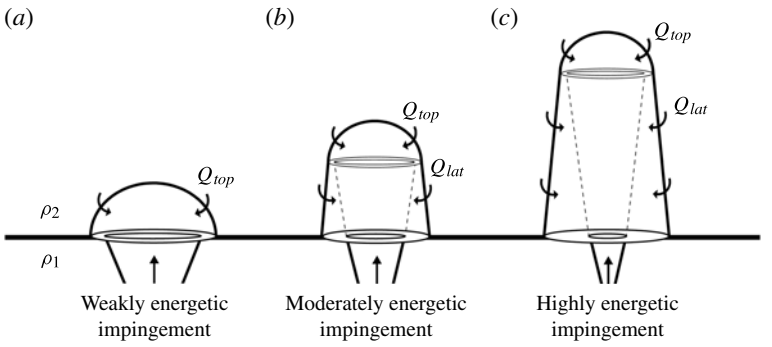

FIGURE 2. Schematic showing the morphology of three flow regimes that we postulate characterise turbulent entrainment across an interface driven by the localised impingement of a jet from below: (*a*) small-Fr_i weakly energetic impingement, in which entrainment into an interfacial dome, atop the incident jet, is dominant; (*b*) intermediate-Fr_i moderately energetic impingement, in which a penetrating fountain entrains both laterally into its downflow and through its top; (*c*) large-Fr_i highly energetic impingement, in which the fountain penetrates a significant distance and lateral entrainment is dominant.

2. Theoretical framework

We examine the steady vertical downward transport of buoyant fluid across a gravitationally stable, horizontal interface (at $z=0$) separating two unbounded miscible fluid masses of uniform densities ρ_1 and $\rho_2 < \rho_1$. The primary transport mechanism is turbulent entrainment, in which energy-containing eddies engulf and advect fluid across the interface. The energetic eddying motions within a localised region of turbulent flow above the interface result from the impingement of a vertically forced, high-Reynolds-number, (quasi-)steady, incompressible, axisymmetric jet of density $\rho_{jet} = \rho_1$. At the density interface, located a distance h above the jet source, the impinging jet has mean radius b_i and mean vertical velocity w_i. The dynamics of turbulent entrainment across the density interface are then governed primarily by the interfacial Froude number

$$\mathrm{Fr}_i = \frac{w_i}{\sqrt{b_i \Delta g'}}, \quad \Delta g' = g\frac{\Delta\rho}{\rho_1}, \Delta\rho = \rho_1 - \rho_2, \tag{2.1}$$

which characterises the relative strengths of the inertial forcing associated with the energy-containing eddies that drive the entrainment and the buoyancy force that acts to stabilise the interface. We focus solely on small density differences $\Delta\rho \ll \rho_1$ so that the Boussinesq approximation is valid. The only constraint we place on h is that it far exceeds the vertical extent of the zone of flow establishment of the jet so the jet may be regarded as fully developed and self-similar on impingement.

When $\Delta g'$ is sufficiently large such that Fr_i is small ($\mathrm{Fr}_i \lesssim 1$), we refer to the impingement as 'weakly energetic'. Weakly energetic impingements also result when h is sufficiently large so that $w_i \propto h^{-1}$ (Fischer *et al.* 1979) is small and $b_i \propto h$ is large. As dense fluid penetrates the interface, strong local buoyancy forces arrest its upward motion, resulting in the formation of a shallow dome-like upwelling, as shown schematically in figure 2(*a*). This behaviour and morphology of flow is confirmed by several experimental studies (Kumagai 1984; Shy 1995; Cotel & Kudo 2008; Hunt & Coffey 2010). Indeed, Hunt & Coffey's (2010) shadowgraph images

(their figure 6) clearly indicate the presence of impingement domes due to small-Fr_i jet–interface interaction. Shy (1995) and Cotel & Breidenthal (1997) deduced from observations that external fluid is turbulently entrained into the impingement dome by strong baroclinic vortices around the periphery of the dome, and is then transported across the interface.

When $\Delta g'$ is sufficiently small such that Fr_i is large ($\mathrm{Fr}_i \gg 1$), we refer to the impingement as 'highly energetic'. The dense fluid carried upwards in the jet penetrates a significant vertical distance (relative to b_i) before retarding buoyancy forces reduce the local vertical momentum flux driving the flow to zero. For $\mathrm{Fr}_i \gg 1$, Baines *et al.* (1993), Lin & Linden (2005) and Ansong, Kyba & Sutherland (2008) identified that the flow above the interface develops as a turbulent fountain comprised of an upflowing jet-like core shrouded by a downflowing plume-like perimeter. The region of flow reversal in the fountain, characterised by a hemispherical cap, is referred to as the 'fountain top' (figure 2*c*). The fountain entrains fluid of density ρ_2 both laterally into its downflow and through its top. The same basic time-averaged picture of the morphology and entrainment also applies to flows with intermediate interfacial Froude numbers that result from 'moderately energetic' impingements (figure 2*b*).

2.1. *Classifying turbulent entrainment across interfaces*

We postulate that turbulent entrainment across an interface resulting from the localised impingement of a turbulent jet can be classified into three regimes, as depicted in figure 2. For weakly energetic impingements producing a shallow penetration (figure 2*a*), the volume flux Q_e entrained across the interface is due solely to the entrainment flux Q_{top} into the interfacial dome atop the incident jet, i.e. $Q_e = Q_{top}$. For highly energetic impingements producing a deep penetration (figure 2*c*), the lateral entrainment flux Q_{lat} into the downflow is expected to be large compared with the fountain top entrainment flux Q_{top}, i.e. $Q_{lat} \gg Q_{top}$. For moderately energetic impingements (figure 2*b*), comparable contributions from Q_{lat} and Q_{top} are anticipated. Thus, the total entrainment flux across the interface can be partitioned as

$$Q_e = Q_{top} + Q_{lat}, \quad \text{where} \quad \begin{cases} Q_{lat} = 0 & \text{for weakly energetic impingements,} \\ Q_{lat} \approx Q_{top} & \text{for moderately energetic impingements,} \\ Q_{lat} \gg Q_{top} & \text{for highly energetic impingements.} \end{cases} \tag{2.2}$$

In § 6 we establish the range of Fr_i for which these distinct regimes occur. An insightful distinction between the two end-member regimes is that, for weakly energetic impingements the localised jet–interface interaction plays an instrumental role in the entrainment dynamics, whereas for highly energetic impingements the interface essentially becomes no more than a reference plane, across which we examine the steady rate of transport of dense fluid.

2.2. *Model development and assumptions*

The dynamics of jet–interface interaction are complex. If one conceptualises the incident jet as being composed of a series of large-scale vortical parcels (Shy 1995), then the impingement of a parcel causes a vertical upward displacement of the interface. Although the two-layer fluid remains close to hydrostatic equilibrium, the 'tilting' of the interface indicates that the surfaces of constant pressure and constant

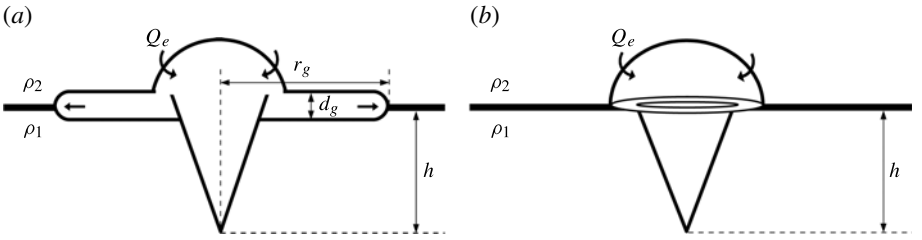

FIGURE 3. Schematic showing: (*a*) $0 < t < \infty$, the impingement dome and interfacial gravity current at some time t after (a weakly energetic) impingement of the jet with the density interface and (*b*) the large-time asymptotic ($t \to \infty$) behaviour, characterised by a two-layer stratification and impingement dome atop the incident jet. The jet source is a distance h below the interface.

density are no longer parallel. The resulting baroclinic torque, which generates vorticity in the opposite sense to the incident vorticity of the impinging parcel, acts to restore the interface back to the horizontal. Shy (1995) showed that the baroclinic vorticity reduces the incident vorticity to zero in a characteristic eddy overturning time $\tau \propto w_i/\Delta g'$. The near-continuous cycle of impacts of these vortical parcels produces vertical oscillations of the interface about its mean position, thus contributing to the generation of interfacial gravity waves. As the wave period ($\propto \sqrt{b_i/\Delta g'}$) is considerably larger than the time scale τ associated with the jet–interface interaction, Cotel & Kudo (2008) reported that these waves do not significantly influence the formation of, or entrainment into, the impingement dome. As a consequence, we do not consider them further here. We note $\sqrt{b_i/\Delta g'} \gg w_i/\Delta g'$ is consistent with $\mathrm{Fr}_i \ll 1$ and thus to jet–interface interaction.

In the region of impingement, the thickness of the interface is controlled by the balance between entrainment into the jet and diffusion (Kaye *et al.* 2010). Neglecting the effects of diffusion, we assume that the interface is infinitesimally thin. Notably, Cotel *et al.* (1997) identified that entrainment into the dome was largely unaffected by any diffusion of the interface.

Fluid entrained from the upper layer spreads radially outwards as a gravity current at the level of the interface, as depicted in figure 3(*a*). Given that we consider an unconfined environment, the spreading of the current is not restricted by vertical boundaries, as is a feature of the aforementioned experimental studies. By balancing the horizontal pressure force driving the current and the retarding inertial force, Ansong *et al.* (2008) show that the depth of the current scales as $d_g \sim t^{-1/2}$ and its radius, measured from the centreline of the jet, scales as $r_g \sim t^{3/4}$. If we take time $t = 0$ as the instant when the jet first impinges on the interface, then at large times the current becomes infinitesimally thin, as depicted in figure 3(*b*). Fluid transport is thereby across the interface. Herein, we consider the unconfined problem in this asymptotic state, thereby allowing us to neglect the time evolution of a stratified intermediate layer, as is considered in confined filling-box models (Kumagai 1984; Cardoso & Woods 1993; Coffey & Hunt 2010). We therefore assume the flow to be quasi-steady so that ρ_1, ρ_2 and h are time-invariant. This enables us to focus our attention solely on Q_e, which is the quantity of primary interest. We first examine small-Fr_i entrainment in § 3 before considering large-Fr_i entrainment in § 5.

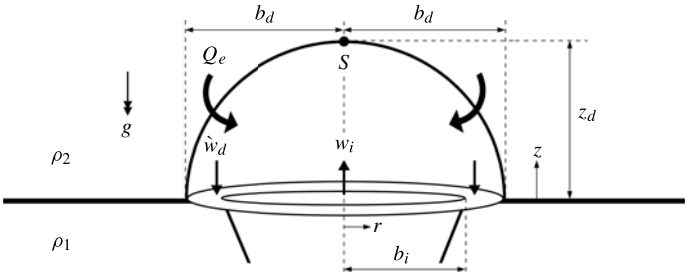

FIGURE 4. Schematic of the time-averaged small-Fr_i axisymmetric semi-ellipsoidal impingement dome resulting from a weakly energetic jet–interface impingement.

3. Theoretical model for small-Fr_i entrainment

Consider the quasi-steady axisymmetric semi-ellipsoidal impingement dome (figure 4), of radius b_d and height z_d, maintained by a turbulent jet of local radius b_i and density $\rho_1 > \rho_2$ at the level of the interface ($z = 0$). In our time-averaged conceptualisation, the volume flux Q_e of buoyant fluid turbulently entrained into the dome from the upper layer is transported downwards across the interface through an annular region of width $(b_d - b_i)$.

3.1. *Conservation equations*

Inspired by the long history of simplified models on turbulent jets and plumes, and indeed in the absence of data to support or justify a more complex variation, top-hat profiles are adopted for the vertical velocity w_i across the jet at the interface (i.e. for $0 \leqslant r \leqslant b_i$, $r = 0$ denoting the vertical axis of the jet) and for the vertical downward velocity $\hat{w}_d < 0$ across the annulus ($b_i \leqslant r \leqslant b_d$). Assuming an incompressible flow, conservation of volume for the dome requires

$$\pi b_i^2 w_i + Q_e = \pi (b_d^2 - b_i^2) w_d, \tag{3.1}$$

where $w_d = |\hat{w}_d|$. Reassuringly, we show (§ 4.2) that the choice of the velocity profile for the jet does not influence the scaling of Q_e. Shy (1995) observed that mixing between the light fluid entrained from the upper layer and the dense jet fluid primarily occurs in a relatively thin layer ($\sim 0.1 b_i$) of strong vorticity at the dome's periphery (cf. figure 5*a*). Moreover, for small-Fr_i flows, we will see (figure 6) that $\pi b_i^2 w_i \gg Q_e$, i.e. fluid added to the dome mainly originates from the jet of density ρ_1. Thus, fluid within the dome predominantly experiences a buoyancy $\Delta g'$ (2.1). Denoting the density of the outflow through the annulus as ρ_d, conservation of vertical momentum for the dome then requires

$$\pi \rho_1 b_i^2 w_i^2 + \pi \rho_d (b_d^2 - b_i^2) w_d^2 = \frac{2\pi}{3} b_d^2 z_d \rho_1 \Delta g', \tag{3.2}$$

where the first and second terms are the fluxes of momentum into and out of the dome, respectively, and the right-hand side is the (downward) buoyancy force acting on the fluid within the dome of volume $(2\pi/3) b_d^2 z_d$. Substituting for w_d from (3.1) into (3.2) gives

$$E_i^2 + 2E_i = \frac{2}{3k^4} \frac{\hat{z}_d^5}{\mathrm{Fr}_i^2} - \frac{2}{3k^2} \frac{\hat{z}_d^3}{\mathrm{Fr}_i^2} - \frac{1}{k^2} \hat{z}_d^2, \tag{3.3}$$

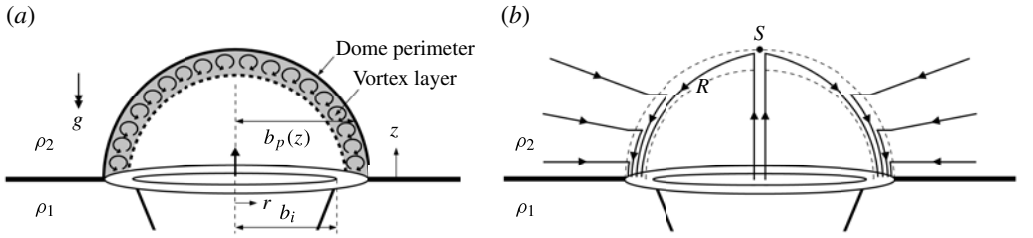

FIGURE 5. Schematics showing: (*a*) the modelled vortex layer (shaded area) of the impingement dome and (*b*) streamlines of the mean flow into the dome.

for Boussinesq flows, where

$$E_i = \frac{Q_e}{\pi b_i^2 w_i}, \quad \hat{z}_d = \frac{z_d}{b_i}, \quad k = \frac{z_d}{b_d}, \tag{3.4a–c}$$

are the dimensionless entrainment flux, the dimensionless penetration depth and the aspect ratio of the dome, respectively. The relationship between these three quantities and the interfacial Froude number Fr_i will be further developed in §§ 3.3–3.4.

3.2. *Entrainment mechanism for the dome*

To close the problem, it is necessary to describe the mechanism by which external fluid of density ρ_2 is turbulently entrained into the impingement dome.

A key distinction may be drawn between the entrainment processes resulting from the interfacial impingement of discrete finite-volume flows (e.g. the vortex rings considered by Linden (1973)) and continuous-flux flows (e.g. our steady jet). Discrete turbulent motions, such as vortex rings and thermals, form an ephemeral impingement dome at the interface. Linden (1973) argued that, upon impingement, the kinetic energy of the vortex ring is first converted into potential energy which is stored temporarily in the distorted interface. As the interface recoils, the stored potential energy is released providing energy for the rebounding vortex ring to entrain buoyant fluid.

In contrast, the localised impingement of a steady turbulent jet with an interface gives rise to a perpetual impingement dome (figure 4). Cotel *et al.* (1997) identified that, owing to the stationarity of the dome, the entrainment process resulting from jet–interface interaction is fundamentally different to the recoil mechanism postulated for a discrete vortex ring. Based on experimental observations, they concluded that the interaction between the incident vorticity within the jet and the baroclinic vorticity generated at the interface, due to its tilting, results in the formation of strong persistent vortices within a relatively thin layer around the perimeter of the dome (see their figure 2). This is consistent with Shy's (1995) observations. Making several rotations whilst remaining almost stationary in space, these baroclinic vortices are predominantly responsible for turbulent entrainment of external fluid into the dome (Cotel & Breidenthal 1997). Accordingly, in developing a mechanistic description of the entrainment, we model the region of strong vorticity at the dome's periphery as a finite-thickness 'vortex' layer whose outermost boundary is the dome perimeter $r = b_p(z)$, as depicted in figure 5(*a*) (the subscript '*p*' reading 'at the perimeter'). In response to the sustained localised vertical forcing of the density interface by the

impinging jet, of horizontal length scale b_i, baroclinic vorticity is generated at a (quasi-)steady rate

$$\frac{\|\boldsymbol{\nabla}\rho \times \boldsymbol{\nabla}P\|}{\rho_1^2} \propto \frac{(\Delta\rho/b_i)(\rho_2 g)}{\rho_1^2} = \frac{\rho_2}{\rho_1}\frac{\Delta g'}{b_i}, \tag{3.5}$$

where P denotes pressure. This (quasi-)steady generation of vorticity maintains the rotational motions within the vortex layer that drive entrainment into the dome. Furthermore, as these baroclinic vortices result from jet–interface interaction, their size is determined primarily by the length scale ($\propto b_i$) of the largest vortical parcels within the impinging jet (Shy 1995). Therefore, at some height z within the vortex layer, a baroclinic vortex that engulfs external fluid at velocity u_e has mean circulation $\Gamma \propto u_e b_i$ and vorticity (i.e. circulation per unit area of the vortex)

$$|\Omega| \propto \frac{\Gamma}{b_i^2} \propto \frac{u_e}{b_i}, \tag{3.6}$$

where the modulus ensures that the entrainment is always into the dome. In our time-averaged picture, the mean vorticity Ω is assumed to vary smoothly over the vertical extent $0 \leqslant z \leqslant z_d$ of the vortex layer. In other words, at any height within the vortex layer, the characteristic vorticity $\Omega(z)$ is regarded as being determined by averaging temporally over the turbulent fluctuations associated with the entrainment process. This is consistent with adopting top-hat profiles for the impinging jet (§ 3.1). Neglecting the effects of viscosity and in the absence of vortex stretching, the vertical component of the steady vorticity equation for the vortex layer is then (Batchelor 1967)

$$\grave{w}_v \frac{\mathrm{d}\Omega}{\mathrm{d}z} = \frac{(\boldsymbol{\nabla}\rho \times \boldsymbol{\nabla}P)_z}{\rho_1^2}, \tag{3.7}$$

where $\grave{w}_v$ is the mean vertical downward velocity within the vortex layer and the right-hand side is the z-component of the baroclinic torque. To estimate the volume flux Q_e of buoyant external fluid entrained into the dome, we seek the mean entrainment velocity $u_e(z)$. Therefore, under the Boussinesq approximation, we relate the steady production of baroclinic vorticity (3.7) to the resulting entrainment velocity (3.6). Taking the constants of proportionality in (3.5) and (3.6) as c_1 and c_2, respectively, the vertical rate of change of u_e is, from (3.7),

$$\frac{\mathrm{d}u_e}{\mathrm{d}z} = \frac{c_1}{c_2}\frac{\Delta g'}{\grave{w}_v}. \tag{3.8}$$

Within the upper layer, a weak inflow towards the dome, as indicated in figure 5(*b*), will be induced as a consequence of entrainment. Within the dome, some dense fluid originating from the jet will reach the top of the dome before reversing direction (figure 5*b*). Notably, the velocity is zero at S, the stagnation point with coordinates ($z = z_d, \quad r = 0$), and accelerations within the dome are proportional to $\Delta g'$ where $\Delta g'/g = \Delta\rho/\rho_1 \ll 1$ for Boussinesq flows. Therefore, assuming that fluid pressures vary hydrostatically and that the surfaces of constant pressure are horizontal, application of Bernoulli's theorem along a streamline within the vortex layer from a point near the top to a height z (cf. streamline R in figure 5*b*) gives

$$u_v^2 + w_v^2 = 2\Delta g'(z_d - z), \tag{3.9}$$

where u_v denotes the horizontal velocity within the vortex layer and $w_v = |\dot{w}_v|$. We note from (3.8) that $\mathrm{d}u_e/\mathrm{d}z < 0$ (as $\dot{w}_v < 0$, $\{c_1, c_2, \Delta g'\} > 0$) and, hence, the entrainment velocity u_e increases monotonically from the stagnation point S to yield its maximum value at the interface ($z = 0$). Moreover, the dome radius b_p increases from zero at S to a maximum value at $z = 0$. Thus, the largest contributions to $Q_e \propto b_p u_e$ are realised near the interface. As the flow is close to vertical here, we assume that $u_v^2/w_v^2 \ll 1$, thereby capturing the dominant velocity component in the region where entrainment is most dominant. This approximation considerably simplifies the analysis, whilst having little effect on the final solution (neglecting u_v^2 reduces our estimate of Q_e by less than 2 %). We substitute for w_v (3.9) into (3.8) and integrate with respect to z. Noting that there is no entrainment into the dome at S, that is $u_e = 0$ at $z = z_d$, we obtain

$$u_e(z) = \alpha w_v(z), \quad \alpha = c_1/c_2 = \text{const.}, \tag{3.10}$$

i.e. the mean horizontal inflow velocity $u_e(z)$ across the boundary between the turbulent flow and the external environment is proportional to the local time-averaged vertical velocity $w_v(z)$ at the dome's periphery. This is consistent with the classic entrainment hypothesis of Morton, Taylor & Turner (1956). Accordingly, the constant of proportionality α in (3.10) is an entrainment coefficient. An appropriate value of α for the downward flow near the dome perimeter is $\alpha = 0.1$ (Turner 1986). Notably, we will see that the exponent n in our entrainment law $E_i \propto \mathrm{Fr}_i^n$ is independent of α and that $E_i \propto \alpha$. At very small Fr_i ($\lesssim 0.1$), entrainment of fluid from the upper layer is primarily driven by local Kelvin–Helmholtz instabilities and the horizontal shear generated by the gravity current propagating below the interface (Ching *et al.* 1993); as we do not account for these processes, our model may break down in this limit. For $0.1 \lesssim \mathrm{Fr}_i \lesssim 1$, entrainment is primarily driven by local energy-containing eddies that engulf external fluid (Linden 1973; Fernando 1991); therefore we expect our model, based on an engulfment mechanism, to capture well the essentials of the entrainment process in this range of interfacial Froude numbers.

As we will now see, this mechanism provides a simple yet effective starting point for quantifying Q_e. The total volume flux entrained from the upper layer into the dome is

$$Q_e = \int_0^{z_d} 2\pi b_p(z) u_e(z)\,\mathrm{d}z = 2\pi\alpha \int_0^{z_d} b_p(z) w_v(z)\,\mathrm{d}z. \tag{3.11}$$

The dome perimeter is the semi-ellipse:

$$\frac{b_p^2(z)}{b_d^2} + \frac{z^2}{z_d^2} = 1, \quad \text{for } z \geqslant 0. \tag{3.12}$$

Substituting for $b_p(z)$ (3.12) and $w_v(z)$ (3.9) into (3.11), and scaling Q_e on $\pi b_i^2 w_i$ gives the dimensionless entrainment flux across the interface as

$$E_i = \frac{Q_e}{\pi b_i^2 w_i} = C\frac{\hat{z}_d^{5/2}}{k\mathrm{Fr}_i}, \quad C = \frac{4\alpha\sqrt{2}}{15}\left(8\sqrt{2} - 7\right). \tag{3.13}$$

As dissipative losses associated with the turbulent interaction at the boundary between the dome and the upper layer have been ignored in the derivation of w_v (3.9), E_i (3.13) represents an upper-bound solution. Having obtained a second independent equation (3.13) relating E_i to the three other dimensionless variables in the problem, namely

Fr_i, $\hat{z}_d$ and k, we now combine the conservation equations (3.3) with our mechanistic entrainment model (3.13). Substituting for k from (3.13) into (3.3) yields the cubic in E_i:

$$2E_i^3 - E_i\left\{3C^2\hat{z}_d^2 + 2C^2\frac{\hat{z}_d^3}{\mathrm{Fr}_i^2} + 3C^4\frac{\hat{z}_d^5}{\mathrm{Fr}_i^2}\right\} - 6C^4\frac{\hat{z}_d^5}{\mathrm{Fr}_i^2} = 0. \tag{3.14}$$

3.3. *Penetration depth of the impingement dome*

To complete our solution we require the variation of $\hat{z}_d = z_d/b_i$ with Fr_i. Given that the penetration of dense fluid and localised entrainment are driven primarily by the kinetic energy of the turbulent motions at the interface (Linden 1973), we proceed by examining the local energetics.

Taking the datum for potential energy as the level ($z = 0$) of the undisturbed interface, the total flux of (solely kinetic) energy $\mathscr{E}_i$ supplied by the jet to the dome and the flux of energy $\mathscr{E}_d$ leaving the dome owing to the outflow through the annulus at $z = 0$ are, respectively,

$$\mathscr{E}_i = \frac{\pi}{2}\rho_1 b_i^2 w_i^3, \quad \mathscr{E}_d = \frac{\pi}{2}\rho_d\left(b_d^2 - b_i^2\right)w_d^3. \tag{3.15a,b}$$

Upon impingement with the interface, some of the energy channelled in the jet is dissipated due primarily to viscous effects, the formation of the dome and in the generation of interfacial gravity waves. For a turbulent plume with Gaussian profiles, Cardoso & Woods (1993) found that the flux of energy dissipated is a constant fraction $\mathscr{F}_G = 0.5$ (the subscript 'G' denoting Gaussian profiles) of the kinetic energy flux supplied at the interface. Accordingly, if a fraction $\mathscr{F}$ of the energy flux $\mathscr{E}_i$ supplied by the impinging jet is dissipated, the flux of energy remaining is $(1 - \mathscr{F})\mathscr{E}_i$. For top-hat profiles $\mathscr{F} = 1/3$ (see appendix A). This available energy is predominantly consumed by the peripheral baroclinic vortices in doing work, at a rate $\mathscr{W}_e$, to turbulently entrain buoyant fluid into the dome. As a consequence of this entrainment, the dome receives a supply of potential energy at a rate $\mathscr{E}_e$. Assuming that the velocity induced in the upper layer is small compared with w_i, we neglect the kinetic energy entrained. Thus, conservation of energy for the dome requires

$$(1 - \mathscr{F})\,\mathscr{E}_i + \mathscr{E}_e = \mathscr{E}_d + \mathscr{W}_e. \tag{3.16}$$

The flux of potential energy entrained into the dome is

$$\mathscr{E}_e = \int_0^{z_d} 2\pi\rho_2 b_p u_e \Delta g' z\,\mathrm{d}z = D\rho_2\Delta g' z_d Q_e, \quad D = \frac{22}{7\sqrt{2}}\left(\frac{\sqrt{2} - 8/11}{8\sqrt{2} - 7}\right). \tag{3.17}$$

For convenience, in (3.17) the potential energy (per unit volume) of a fluid parcel in the upper layer (density ρ_2) is calculated relative to the potential energy (per unit volume) of a fluid parcel in the lower layer (density ρ_1), i.e. we consider reduced potential energies that scale with $\Delta g'$. Given that $Q_e = Q_d - Q_i$ (3.1), where $Q_d = \pi(b_d^2 - b_i^2)w_d$ and $Q_i = \pi b_i^2 w_i$, substituting for $\mathscr{E}_i$, $\mathscr{E}_d$ (3.15) and $\mathscr{E}_e$ (3.17) into the energy conservation equation (3.16) yields

$$Q_i\left\{(1 - \mathscr{F})\frac{w_i^2}{2} - D\Delta g' z_d\right\} = Q_d\left\{\frac{w_d^2}{2} + \frac{\mathscr{W}_e}{\rho_1 Q_d} - D\Delta g' z_d\right\}, \tag{3.18}$$

for Boussinesq flows. The left-hand side of (3.18) describes, for the penetrating upward flow, the conversion of the supplied kinetic energy into potential energy within the dome; the expression within the parenthesis is synonymous with the Bernoulli equation. The right-hand side of (3.18) describes, for the downward flow, the conversion of potential energy, gained from the work done in entrainment, into kinetic energy of the outflow from the dome. Drawing an analogy with Bernoulli's theorem, we seek a solution to (3.18) of the form

$$Q_i\left\{(1-\mathscr{F})\,\frac{w_i^2}{2}-D\Delta g' z_d\right\}=Q_d\left\{\frac{w_d^2}{2}+\frac{\mathscr{W}_e}{\rho_1 Q_d}-D\Delta g' z_d\right\}=\text{const.} \tag{3.19}$$

As there is no penetration ($z_d=0$) into the upper layer when the kinetic energy supplied by the jet is zero ($w_i^2=0$), (3.19) gives the penetration depth of the dome as

$$\hat{z}_d=\frac{z_d}{b_i}=B\mathrm{Fr}_i^2,\quad B=\frac{1}{3D}\approx 0.94. \tag{3.20}$$

From (3.20), we note that $\hat{z}_d$ is independent of α, a result one would expect on physical grounds. The $\hat{z}_d\propto \mathrm{Fr}_i^2$ relationship derived is consistent with previous experimental results and theoretical arguments for interfacial domes (Linden (1973); Ching *et al.* (1993); Shy (1995); Cotel *et al.* (1997)). Moreover, this scaling is evident on considering the relevant velocity and time scales. We recall (§ 2.2) that the baroclinic vorticity reduces the incident vorticity of an impinging eddy to zero in a time scale $\tau\sim w_i/\Delta g'$. Thus, the eddy attains a height $z_d\propto w_i\tau$, i.e. $z_d/b_i\sim \mathrm{Fr}_i^2$.

3.4. *Theoretical solution for E_i*

With the problem fully closed, we substitute for $\hat{z}_d$ (3.20) into (3.14). This yields a cubic in the dimensionless entrainment flux E_i as a function solely of the interfacial Froude number:

$$E_i^3-a_1E_i-a_2=0, \tag{3.21}$$

with coefficients

$$a_1=\tfrac{3}{2}C^2B^2\mathrm{Fr}_i^4\left(1+\tfrac{2}{3}B+C^2B^3\mathrm{Fr}_i^4\right),\quad a_2=3C^4B^5\mathrm{Fr}_i^8. \tag{3.22a,b}$$

This cubic has only one positive root given by

$$E_i=\left\{\frac{a_2}{2}+\sqrt{\left(\frac{a_2}{2}\right)^2-\left(\frac{a_1}{3}\right)^3}\right\}^{1/3}+\left\{\frac{a_2}{2}-\sqrt{\left(\frac{a_2}{2}\right)^2-\left(\frac{a_1}{3}\right)^3}\right\}^{1/3}. \tag{3.23}$$

For small Fr_i, a two-step procedure reduces (3.23) to a simple power law that closely approximates the full analytic solution. First, given $C\approx 0.16$ (3.13) and $B\approx 0.94$ (3.20), we find that the third term within the parenthesis of (3.22*a*) is sufficiently small compared with $2B/3$ such that it may be neglected when $\mathrm{Fr}_i\ll(2/(3C^2B^2))^{1/4}\approx 2.3$. Second, upon examining the relative magnitudes of the two terms $((a_2/2)^2,\,(a_1/3)^3)$ within the square root in (3.23), we find that

$$\frac{(a_2/2)^2}{(a_1/3)^3}=\frac{27a_2^2}{4a_1^3}\ll 1\quad\text{for } \mathrm{Fr}_i\ll\left(\frac{1+2B/3}{18C^2B^4}\right)^{1/4}\approx 1.4. \tag{3.24}$$

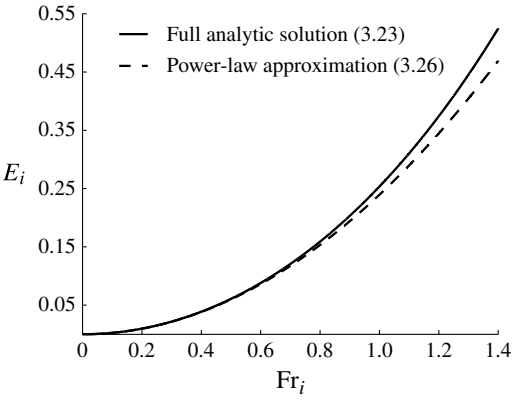

FIGURE 6. Small-Fr_i entrainment law. Entrainment flux E_i as a function of the interfacial Froude number Fr_i. The solid line is our full analytic solution (3.23) and the dashed line is our approximate power law $E_i = 0.24\mathrm{Fr}_i^2$ (3.26).

Restricting our attention to $\mathrm{Fr}_i \ll 1.4$, we may simplify the full analytic solution (3.23) to

$$E_i = \mathbb{R}\left\{\sqrt{\frac{a_1}{3}}\left(\mathrm{i}^{1/3} + (-\mathrm{i})^{1/3}\right)\right\}, \quad \begin{cases} \mathrm{i}^{1/3} = \{-\mathrm{i},\ (\sqrt{3}+\mathrm{i})/2,\ (-\sqrt{3}+\mathrm{i})/2\}, \\ (-\mathrm{i})^{1/3} = \{\mathrm{i},\ (-\sqrt{3}-\mathrm{i})/2,\ (\sqrt{3}-\mathrm{i})/2\}, \end{cases} \tag{3.25a,b}$$

where $\mathrm{i} = \sqrt{-1}$. The only solutions for $\mathrm{i}^{1/3}$ and $(-\mathrm{i})^{1/3}$ that yield real, positive values of E_i are $\mathrm{i}^{1/3} = (\sqrt{3}+\mathrm{i})/2$ and $(-\mathrm{i})^{1/3} = (\sqrt{3}-\mathrm{i})/2$. Therefore, from (3.25),

$$E_i = A\mathrm{Fr}_i^2, \quad A = BC\sqrt{B+\tfrac{3}{2}} \approx 0.24, \quad \text{for } \mathrm{Fr}_i \ll 1.4. \tag{3.26}$$

Thus, our solution for E_i is in the form of the entrainment law $E_i = A\mathrm{Fr}_i^n$ (1.1) proposed by Turner (1968), with an exponent of $n = 2$.

4. Analysis of model predictions for small-Fr_i flows

4.1. *An entrainment law*

Figure 6 plots the full analytic solution (3.23). Also plotted is the power-law $E_i = A\mathrm{Fr}_i^2$ (3.26) approximation to this. Evidently, the quadratic entrainment law closely approximates the full solution for $\mathrm{Fr}_i \lesssim 1$; note that the two solutions are graphically indistinguishable for $\mathrm{Fr}_i \lesssim 0.7$. Although the power law diverges from the full solution for $\mathrm{Fr}_i > 1$, the difference between the two solutions remains less than 10 % at $\mathrm{Fr}_i = 1.4$. Indeed, we will see in § 4.3 that 'small-Fr_i' flows are realised for $\mathrm{Fr}_i < 1.4$.

Our quadratic result $E_i \propto \mathrm{Fr}_i^2$ is in accordance with several previous studies (Linden 1975; Cardoso & Woods 1993; Ching *et al.* 1993) and also a significant subset of Kumagai's (1984) data (see figure 12*a* where this data is replotted). Notably, Kumagai reports that $0.1 < A < 0.25$ and Zilitinkevich (1991) shows in his review that $0.1 \lesssim A \lesssim 0.3$. Hence, our value of $A = 0.24$ is also well supported. In § 7 we show that our small-Fr_i entrainment law (3.26) agrees very well with Kumagai's measurements. Given that $C \sim \alpha$ (3.13), a reduction in α of 15 % from $\alpha = 0.1$ to $\alpha = 0.085$ (which is towards the lower end of the reported values of α (Kaye & Hunt 2006)) decreases

A from $A \approx 0.24$ to $A \approx 0.2$ (3.26); crucially, as $E_i \sim \alpha$ (3.26), the functional form of our power law is unchanged. Similarly, E_i is not highly sensitive to changes in $\mathscr{F}$ (see appendix A).

4.2. *The mechanics of our small-*Fr_i *entrainment law*

We now elucidate the dominant physics at the heart of our quadratic entrainment law approximation by presenting complementary scaling arguments based on the jet–interface interaction. In a baroclinic eddy overturning time scale τ (see § 2.2), the impinging jet supplies a mass $\rho_1 Q_i \tau$ of turbulent fluid, with mean vertical velocity w_i, causing a vertical deflection of the interface. Local baroclinic vortices, formed due to the tilting of the interface, extract a fraction of the kinetic energy supplied by the jet, a supply which scales as

$$\mathrm{KE}_i \sim \rho_1 Q_i \tau w_i^2. \tag{4.1}$$

Given that the flow under consideration is steady, in the same time scale τ the extracted energy is expended by the vortices in doing work to entrain a mass $\rho_2 Q_e \tau$ of fluid from the upper layer against the buoyancy contrast $\Delta g'$, and over a distance proportional to the length scale of interfacial turbulence, b_i. Thus, the work done in the entrainment process scales as

$$W_e \sim \rho_2 Q_e \tau \Delta g' b_i. \tag{4.2}$$

Invoking a work–energy balance ($W_e \propto \mathrm{KE}_i$) yields, for Boussinesq flows,

$$\frac{Q_e}{b_i^2 w_i} \sim \frac{w_i^2}{b_i \Delta g'} = \mathrm{Fr}_i^2. \tag{4.3}$$

Thus, our quadratic power-law captures an energy balance; the entrainment rate increases as the supply of energy increases relative to the energy required for downward transport of buoyant fluid.

To illustrate the work–energy balance ($W_e \propto \mathrm{KE}_i$), we examine the actual magnitudes of the dimensionless flux of (available) kinetic energy $(1-\mathscr{F})\tilde{\mathscr{E}}_i = (1-\mathscr{F})\mathscr{E}_i/\mathscr{E}_{sc}$ and the dimensionless work rate for entrainment $\tilde{\mathscr{W}}_e = \mathscr{W}_e/\mathscr{E}_{sc}$ (the subscript '*sc*' reading 'scale'). Here, the energy flux scale $\mathscr{E}_{sc} = \pi \rho_1 b_i^2 w_i^3 / 2\mathrm{Fr}_i^3$ is formed by taking the velocity scale as $\sqrt{\Delta g' b_i}$ and the length scale as b_i. It is also insightful to consider the dimensionless energy flux $\tilde{\mathscr{E}}_e = \mathscr{E}_e/\mathscr{E}_{sc}$ entrained into the dome. From (3.15), (3.16) and (3.17),

$$\left.\begin{gathered} (1-\mathscr{F})\tilde{\mathscr{E}}_i = \frac{2}{3}\mathrm{Fr}_i^3, \quad \tilde{\mathscr{E}}_e = \frac{2}{3}E_i \mathrm{Fr}_i^3, \\ \tilde{\mathscr{E}}_d = \left(\frac{b_d^2}{b_i^2} - 1\right)\frac{w_d^3}{w_i^3}\mathrm{Fr}_i^3, \quad \tilde{\mathscr{W}}_e = (1-\mathscr{F})\tilde{\mathscr{E}}_i + \tilde{\mathscr{E}}_e - \tilde{\mathscr{E}}_d, \end{gathered}\right\} \tag{4.4}$$

where $\tilde{\mathscr{E}}_d = \mathscr{E}_d/\mathscr{E}_{sc}$. To plot these energy fluxes, we evaluate w_d/w_i using (3.2) and b_d/b_i from $(b_d/z_d)(z_d/b_i) = B\mathrm{Fr}_i^2/k$, where k is calculated from (3.13). Figure 7(*a*) plots $(1-\mathscr{F})\tilde{\mathscr{E}}_i$, $\tilde{\mathscr{E}}_e$ and $\tilde{\mathscr{W}}_e$ (4.4) as a function of Fr_i. Evidently, the majority of the (available) kinetic energy is expended in doing work to entrain buoyant fluid into the dome. However, the gain in energy flux $\tilde{\mathscr{E}}_e$ within the dome, as a result of the entrainment, is relatively small for $\mathrm{Fr}_i \ll 1$ as $\tilde{\mathscr{E}}_e \propto \mathrm{Fr}_i^5$ (4.4). Plotting $\tilde{\mathscr{W}}_e$ against $(1-\mathscr{F})\tilde{\mathscr{E}}_i$ in figure 7(*b*), we find that the work rate for entrainment scales linearly on the kinetic energy flux supplied, following $\tilde{\mathscr{W}}_e \approx 0.46(1-\mathscr{F})\tilde{\mathscr{E}}_i$; this is in accord with our scaling arguments (4.3). Thus, just under one-half of the available energy is consumed in entrainment.

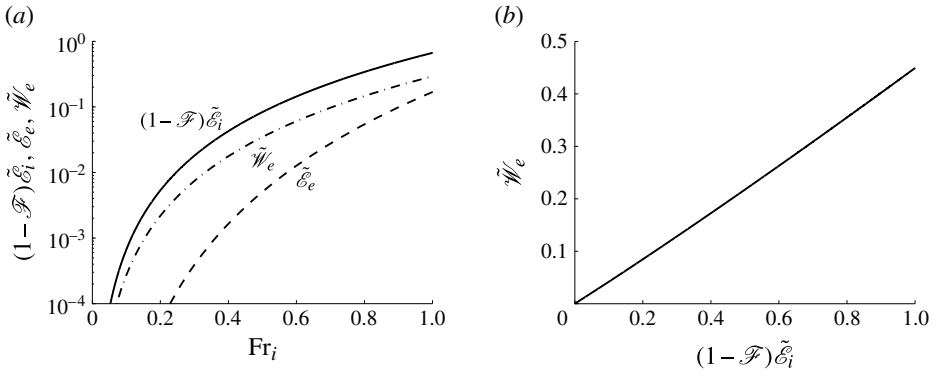

FIGURE 7. (*a*) Kinetic energy flux $(1-\mathscr{F})\tilde{\mathscr{E}}_i$ available for entrainment (solid line), work rate for entrainment $\tilde{\mathscr{W}}_e$ (dashed-dotted line) and flux of energy $\tilde{\mathscr{E}}_e$ entrained into the dome (dashed line) as a function of Fr_i. (*b*) Work rate $\tilde{\mathscr{W}}_e$ against (available) kinetic energy flux $(1-\mathscr{F})\tilde{\mathscr{E}}_i$.

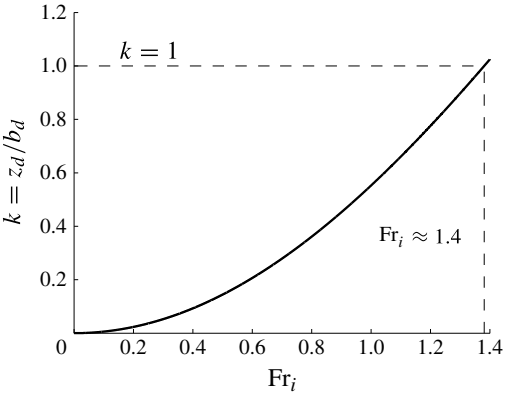

FIGURE 8. Aspect ratio $k = z_d/b_d$ of the impingement dome as a function of Fr_i. The dashed lines show that $k = 1$ (i.e. the dome is a hemisphere) when $\mathrm{Fr}_i = 1.381 \approx 1.4$.

4.3. *An upper bound on* Fr_i *for small-*Fr_i *entrainment*

The range of Fr_i that may be regarded as 'small' is evident upon examining the aspect ratio $k = z_d/b_d$ of the impingement dome. Using the full solution (3.23) for E_i in (3.13), we plot the variation of k with Fr_i in figure 8. Evidently, $k \ll 1$ for $\mathrm{Fr}_i \ll 1$ and, hence, these impingements produce no more than a shallow penetration, resulting in flat, relatively wide domes. Notably, domes of comparable width and penetration depth ($k \sim 1$) result when the rise velocity of the dense fluid exceeds the opposing buoyancy-induced velocity, i.e. for $\mathrm{Fr}_i > 1$.

For sufficiently energetic impingements, the jet penetrates as a dense fountain whose aspect ratio exceeds unity, i.e. $k > 1$. Moreover, as highly forced fountains ($\mathrm{Fr}_i \gg 1$) exhibit a jet-like behaviour over a majority of their rise height (Turner 1966; Kaye & Hunt 2006), $k \gg 1$. Following these arguments, we regard $k = 1$ as marking the transition from a flow described by an impingement dome ($k < 1$, shallow penetration) to a flow described by a fountain ($k > 1$, deep penetration). Accordingly, from figure 8, small-Fr_i flows are realised for $\mathrm{Fr}_i < 1.4$.

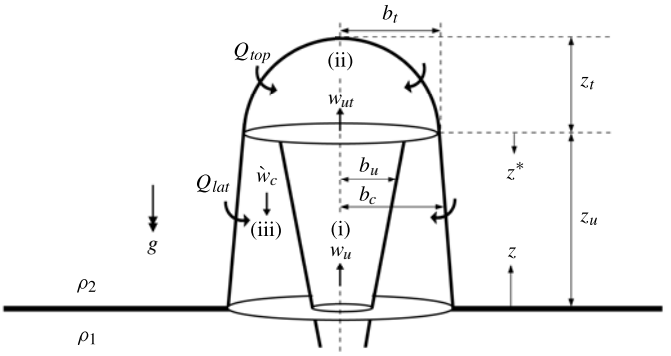

FIGURE 9. Schematic and notation for the time-averaged turbulent fountain which forms in the upper layer for moderately or highly energetic (i.e. $\mathrm{Fr}_i > 1.4$) interfacial impingements. The fountain is characterised by three regions: (i) an upflow, (ii) fountain top and (iii) counterflow. The total entrainment flux across the interface is the sum of the fountain top (Q_{top}) and lateral (Q_{lat}) entrainment fluxes. In our model, the total fountain width $2b_c$ is assumed constant with height.

5. Theoretical model of high Fr_i (penetrative) entrainment

When $\mathrm{Fr}_i > 1.4$, the impingement is assumed to be sufficiently energetic that the jet develops as a fully penetrating turbulent fountain in the upper layer. Indeed, Baines *et al.* (1993) and Lin & Linden (2005) confirm that at relatively large Fr_i ($\gtrsim 1.5$), the interfacial impingement of a vertically forced shear flow gives rise to a penetrating fountain.

We model the fountain by considering three flow regions that characterise its behaviour (figure 9): (i) a negatively buoyant upflowing jet-like core of density $\rho_u(z) > \rho_2$, (ii) a fountain top where the flow reverses direction and (iii) an annular negatively buoyant counterflowing plume-like flow of density $\rho_c(z) > \rho_2$ (the subscripts 'u' and 'c' denoting 'upflow' and 'counterflow', respectively). Within the upflow and counterflow, top-hat profiles are adopted to describe the time-averaged horizontal variation of vertical velocities, w_u and $\dot{w}_c < 0$, and buoyancies

$$g'_u = g\left(\frac{\rho_u - \rho_2}{\rho_1}\right), \quad g'_c = g\left(\frac{\rho_c - \rho_2}{\rho_1}\right). \tag{5.1a,b}$$

At the lateral boundary between the fountain and the upper layer, large-scale eddies turbulently engulf external fluid into the counterflow, giving rise to a lateral entrainment flux Q_{lat}. Turbulent entrainment also maintains a continuous exchange of fluxes between the two counterflowing streams. Following Bloomfield & Kerr (2000), we assume that the upward (w_u) and downward ($\dot{w}_c$) velocities drive entrainment into the upflow and counterflow, respectively. Given that the fountain core exhibits jet-like behaviour ($w_u \gg |\dot{w}_c|$ for a significant fraction of the upflow's rise height z_u, figure 9), it is reasonable to neglect the entrainment of fluid from the upflow into the counterflow. This assumption, which simplifies the analysis, is also consistent with the results of numerical simulations of forced fountains performed by Williamson, Armfield & Lin (2011). However, as the supply of dense fluid to the counterflow is reduced (by neglecting entrainment from the upflow), our model is likely to underestimate the density ρ_c of the counterflow, i.e. the upflow becomes shrouded

by a lighter counterflow, thus giving rise to lower-bound solutions for z_u and, as a consequence, Q_{lat}. In addition, guided by the measurements of Mizushina *et al.* (1982), the total fountain width $2b_c$ is assumed constant with height. Based on these assumptions, a model of the penetrating fountain is now developed to predict, for $\mathrm{Fr}_i > 1.4$, the entrainment flux Q_e across the interface and its components, the lateral (Q_{lat}) and fountain top (Q_{top}) entrainment fluxes.

5.1. *Upflowing jet core*

The fluxes of volume, momentum and buoyancy that are entrained per unit height into the upflow are $2\pi b_u u_{eu}$, $2\pi\rho_c b_u \grave{w}_c u_{eu}$ and $2\pi b_u u_{eu} g'_c$, respectively. Here b_u is the upflow radius and u_{eu} the entrainment velocity. Following Morton *et al.* (1956), conservation of volume flux ($\pi b_u^2 w_u$), specific momentum flux ($\pi b_u^2 w_u^2$) and buoyancy flux ($\pi b_u^2 w_u g'_u$) for the upflow require

$$\frac{\mathrm{d}}{\mathrm{d}z}(\pi b_u^2 w_u) = 2\pi b_u(\alpha_u w_u), \quad \frac{\mathrm{d}}{\mathrm{d}z}(\pi b_u^2 w_u^2) = -\pi b_u^2 g'_u - 2\pi b_u w_c(\alpha_u w_u), \tag{5.2a,b}$$

$$\frac{\mathrm{d}}{\mathrm{d}z}(\pi b_u^2 w_u g'_u) = 2\pi b_u g'_c(\alpha_u w_u), \tag{5.3}$$

where $\alpha_u = u_{eu}/w_u$ is the top-hat entrainment coefficient for the upflowing jet core and $w_c = |\grave{w}_c|$. Herein, we take $\alpha_u = 0.07$ (Fischer *et al.* 1979). Scaling quantities of interest on their values at the interface (i.e. the fountain source), for the upflow we seek the vertical variation of its dimensionless radius β_u, dimensionless vertical velocity ω_u and Froude number Fr_u. Accordingly, we introduce

$$\beta_u = \frac{b_u}{b_i}, \quad \omega_u = \frac{w_u}{w_i}, \quad \mathrm{Fr}_u = \frac{w_u}{\sqrt{b_u g'_u}}, \quad \xi = \frac{6\alpha_u}{5}\frac{z}{b_i}. \tag{5.4a–d}$$

The vertical coordinate z is scaled on $5b_i/(6\alpha_u)$ so that in the absence of a counterflow, we recover the non-dimensional conservation equations of Kaye & Hunt (2006). For the counterflow, the dimensionless radius β_c, dimensionless vertical velocity ω_c and Froude number Fr_c are

$$\beta_c = \frac{b_c}{b_i}, \quad \omega_c = \frac{w_c}{w_i}, \quad \mathrm{Fr}_c = \frac{w_c}{\sqrt{b_a g'_c}}, \tag{5.5a–c}$$

where $b_a = \sqrt{b_c^2 - b_u^2}$ is the characteristic width of the annulus. In dimensionless form the conservation equations become

$$\frac{\mathrm{d}}{\mathrm{d}\xi}\left(\beta_u^2\omega_u\right) = \frac{5}{3}\beta_u\omega_u, \quad \frac{\mathrm{d}}{\mathrm{d}\xi}\left(\beta_u^2\omega_u^2\right) = -\frac{5}{6\alpha_u}\frac{\beta_u\omega_u^2}{\mathrm{Fr}_u^2} - \frac{5}{3}\beta_u\omega_u\omega_c, \quad \frac{\mathrm{d}}{\mathrm{d}\xi}\left(\frac{\beta_u\omega_u^3}{\mathrm{Fr}_u^2}\right) = \frac{5}{3}\frac{\beta_u\omega_u\omega_c^2}{\beta_a\mathrm{Fr}_c^2}, \tag{5.6a–c}$$

where $\beta_a = b_a/b_i$. Differentiating the terms within the parentheses of (5.6) and, after considerable manipulation, the non-dimensional governing equations for the upflow take the form

$$\frac{\mathrm{d}\beta_u}{\mathrm{d}\xi} = \frac{5}{3}\left(1 + \frac{1}{4\alpha_u}\frac{1}{\mathrm{Fr}_u^2}\right) + I_1, \quad \frac{\mathrm{d}\omega_u}{\mathrm{d}\xi} = -\frac{5}{3}\frac{\omega_u}{\beta_u}\left(1 + \frac{1}{2\alpha_u}\frac{1}{\mathrm{Fr}_u^2}\right) + I_2, \tag{5.7a,b}$$

$$\frac{\mathrm{d}\mathrm{Fr}_u}{\mathrm{d}\xi} = -\frac{5}{3}\frac{\mathrm{Fr}_u}{\beta_u}\left(1 + \frac{5}{8\alpha_u}\frac{1}{\mathrm{Fr}_u^2}\right) + I_3, \tag{5.8}$$

where the 'interaction' terms

$$I_1 = \frac{5}{6}\frac{\omega_c}{\omega_u}, \quad I_2 = -\frac{5}{3}\frac{\omega_c}{\beta_u}, \quad I_3 = -\frac{5}{3}\frac{\mathrm{Fr}_u}{\beta_u}\frac{\omega_c}{\omega_u}\left(\frac{5}{4} + \frac{1}{2}\frac{\omega_c\beta_u\mathrm{Fr}_u^2}{\omega_u\beta_a\mathrm{Fr}_c^2}\right) \tag{5.9a–c}$$

account for entrainment into the upflow and into the counterflow. In the absence of a counterflow $I_1 = I_2 = I_3 = 0$ and, thus, (5.7) and (5.8) reduce to the classic plume equations (albeit with negative buoyancy). The starting (source) conditions for the upflow are

$$\beta_u(\xi = 0) = 1, \quad \omega_u(\xi = 0) = 1, \quad \mathrm{Fr}_u(\xi = 0) = \mathrm{Fr}_i. \tag{5.10a–c}$$

5.2. *Flow reversal region: fountain top*

Dense fluid, depleted of its (source) momentum flux, reverses direction near the top of the fountain. Notably, as the buoyancy force is dominant in this region of flow reversal, the local buoyancy velocity exceeds the upflow velocity. We recall (§ 4.3) that the interfacial dome atop the impinging jet (figure 2*a*) takes the form of a hemisphere ($k = 1$) when $\mathrm{Fr}_i \approx 1.4$ (figure 8). Akin to an interfacial dome, the top of the penetrating fountain (cf. figure 2*c*) is characterised by a buoyancy-dominated cap-like structure into which external fluid is turbulently entrained. Drawing on these similarities, we model the flow reversal region as a hemispherical dome (the fountain top), forming at a height $z = z_u$ where the upflow Froude number takes a local value $\mathrm{Fr}_u = \mathrm{Fr}_{ut} = 1.4$ (the subscript 't' signifying the fountain top). Following the conservation arguments for the interfacial dome developed in § 3.1, conservation of volume and of momentum for the fountain top, of width and height b_t, require

$$\pi b_{ut}^2 w_{ut} + Q_{top} = \pi(b_t^2 - b_{ut}^2)w_t, \quad \pi\rho_{ut}b_{ut}^2w_{ut}^2 + \pi\rho_t(b_t^2 - b_{ut}^2)w_t^2 = \frac{2\pi}{3}\rho_{ut}g'_{ut}b_t^3, \tag{5.11a,b}$$

where b_{ut}, w_{ut}, ρ_{ut} and g'_{ut} are the radius, vertical velocity, density and buoyancy, respectively, of the upflow at $z = z_u$ and w_t the magnitude of the vertical downward velocity of the outflow from the fountain top. Substituting for w_t^2 from (5.11*a*) into (5.11*b*) and writing $g'_{ut} = w_{ut}^2/(b_{ut}\mathrm{Fr}_{ut}^2)$ from (5.4) yields a polynomial in the dimensionless fountain top radius $\beta_t = b_t/b_i$:

$$\frac{2\beta_t^5}{\mathrm{Fr}_{ut}^2\beta_{ut}^5} - \frac{2\beta_t^3}{\mathrm{Fr}_{ut}^2\beta_{ut}^3} - \frac{3\beta_t^2}{\beta_{ut}^2} - 3E_{ut}(E_{ut} + 2) = 0, \quad E_{ut} = \frac{Q_{top}}{\pi b_{ut}^2 w_{ut}}, \tag{5.12}$$

where $\beta_{ut} = b_{ut}/b_i$. The fountain top entrainment flux is determined by Fr_{ut}. Given $E_i = 0.525$ when $\mathrm{Fr}_i = 1.4$ (3.23), we take $E_{ut} = 0.525$ for $\mathrm{Fr}_{ut} = 1.4$. As lateral entrainment is dominant at large Fr_i, the choice of Fr_{ut} has a relatively minor influence on the total entrainment flux E_i in this regime. Our model is relatively insensitive to the choice of Fr_{ut}, even at low Fr_i. For example, decreasing $\mathrm{Fr}_{ut} = 1.4$ to $\mathrm{Fr}_{ut} = 1.2$ results in a less than 7 % reduction in E_i for $\mathrm{Fr}_i > 4$ (large Fr_i); for $1.4 < \mathrm{Fr}_i < 4$, where fountain top entrainment provides a significant contribution to E_i, the reduction in E_i is no greater than 15 %.

The dimensionless vertical velocity of the outflow from the fountain top is, from (5.11*b*),

$$\omega_t = \frac{w_t}{w_i} = \omega_{ut}\left\{\frac{2\beta_t^3 - 3\beta_{ut}^3\mathrm{Fr}_{ut}^2}{3\beta_{ut}\mathrm{Fr}_{ut}^2(\beta_t^2 - \beta_{ut}^2)}\right\}^{1/2}. \tag{5.13}$$

5.3. *Counterflow*

To complete our model, it is necessary to describe the counterflow. Following Morton *et al.* (1956), conservation of volume for the counterflow requires

$$\frac{\mathrm{d}}{\mathrm{d}z^*}[\pi(b_c^2 - b_u^2)w_c] = 2\pi b_c(\alpha_c w_c) - 2\pi b_u(\alpha_u w_u), \tag{5.14}$$

where z^* $(=z_u - z)$ is the vertical downward coordinate with origin at the base of the fountain top (figure 9) and α_c the entrainment coefficient for the counterflow. Numerical simulations performed by Williamson *et al.* (2011) suggest $0.1 < \alpha_c < 0.2$. Treating the counterflow as a line plume, Bloomfield & Kerr (2000) choose $\alpha_c = 0.147$. Herein, we take $\alpha_c = 0.15$, the mid-value of the range of Williamson *et al.* (2011). Mizushina *et al.* (1982) found that the total fountain width, $2b_c$, is approximately constant with height. Accordingly, we non-dimensionalise (5.14) and invoke the simplifying assumption that $\mathrm{d}b_c/\mathrm{d}z = 0$ to obtain

$$\frac{\mathrm{d}\omega_c}{\mathrm{d}\xi^*} = \frac{5}{3\left(\beta_c^2 - \beta_u^2\right)}\left\{\frac{\alpha_c}{\alpha_u}\beta_c\omega_c - \beta_u\omega_u + \frac{6}{5}\beta_u\omega_c\frac{\mathrm{d}\beta_u}{\mathrm{d}\xi^*}\right\}, \quad \beta_c(\xi^*) = \beta_t, \tag{5.15a,b}$$

where $\xi^* = (6\alpha_u/5)z^*/b_i$. The starting condition for (5.15) is $\omega_c(\xi^* = 0) = \omega_t$, with ω_t given by (5.13). Finally, conservation of buoyancy over the total width $2b_c$ of the fountain requires

$$\pi(b_c^2 - b_u^2)w_c g_c' = \pi b_u^2 w_u g_u', \quad \text{i.e. } \mathrm{Fr}_c = \mathrm{Fr}_u\left\{\frac{\omega_c^3\sqrt{\beta_t^2 - \beta_u^2}}{\omega_u^3\beta_u}\right\}^{1/2}. \tag{5.16}$$

At this stage, it is useful to highlight key differences between our new fountain model and the model of Bloomfield & Kerr (2000). We characterise the flow reversal region as a hemispherical dome and account for fountain top entrainment, whereas these features are not considered by Bloomfield & Kerr (2000). In addition, we have assumed that the total fountain width is invariant with height and that entrainment from the upflow into the counterflow is negligible.

Solutions for E_i were obtained using an iterative procedure. First, in the absence of a counterflow ($I_1 = I_2 = I_3 = 0$), the upflow equations, (5.7) and (5.8), were solved using a fourth-order Runge–Kutta finite-difference scheme. This gave the radius β_{ut} and vertical velocity ω_{ut} of the upflow at height $\xi = \xi_u$, where $\mathrm{Fr}_u = 1.4$. The width β_c (5.12) and starting vertical velocity ω_t (5.13) of the counterflow were then calculated. The counterflow equations, (5.15) and (5.16), were solved to obtain $\omega_c(\xi^*)$ and $\mathrm{Fr}_c(\xi^*)$. These values of β_c, ω_c and Fr_c were used in the next numerical integration of the upflow equations. This procedure was repeated until E_i converged to a fixed value. The total entrainment flux E_i and its two components, namely the fountain top $E_{i,top} = Q_{top}/Q_i$ and lateral $E_{i,lat} = Q_{lat}/Q_i$ entrainment fluxes, were determined from

$$E_i = E_{i,top} + E_{i,lat}, \quad E_{i,top} = E_{ut}\beta_{ut}^2\omega_{ut}, \quad E_{i,lat} = \frac{5}{3}\frac{\alpha_c}{\alpha_u}\int_0^{\xi_u}\beta_c\omega_c\,\mathrm{d}\xi^*. \tag{5.17a–c}$$

6. Theoretical predictions and analysis of results

Figure 10 plots the full predicted variation of E_i with Fr_i encompassing the dynamics of the three regimes we identify (small, intermediate and large Fr_i). For $\mathrm{Fr}_i < 1.4$, E_i is given by the analytic solution (3.23) for entrainment flux into the

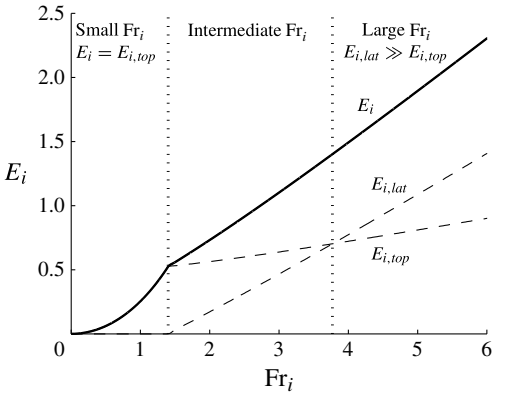

FIGURE 10. Entrainment flux E_i (solid line) as a function of the interfacial Froude number Fr_i. For $\mathrm{Fr}_i < 1.4$, E_i is given by (3.23) and for $\mathrm{Fr}_i > 1.4$, E_i is obtained by numerically solving (5.7) and (5.8). The vertical dotted lines mark the boundaries between the three entrainment regimes. The dashed lines are the lateral and fountain top entrainment fluxes, $E_{i,lat}$ and $E_{i,top}$, where $E_i = E_{i,top} + E_{i,lat}$.

impingement dome; in this small-Fr_i regime, $E_i \propto \mathrm{Fr}_i^2$ (3.26). For $\mathrm{Fr}_i \geqslant 1.4$, E_i is obtained from our fountain model of § 5. A curve of best fit to our numerical solution (figure 12*b*) reveals that

$$E_i = A\mathrm{Fr}_i, \quad A \approx 0.42, \quad \text{for } \mathrm{Fr}_i > 3.8. \tag{6.1}$$

Thus, our large-Fr_i entrainment law is of the form $E_i = A\mathrm{Fr}_i^n$ proposed by Turner (1968), with $n = 1$. This linear power law for $\mathrm{Fr}_i \gg 1$ is consistent with the results of Baines *et al.* (1993).

6.1. *Relative contributions of top and lateral entrainment*

To assist with the interpretation of the entrainment regimes, figure 10 plots the components $E_{i,top}$ and $E_{i,lat}$ (5.17) that comprise E_i. Weakly energetic impingements which occur for $0 < \mathrm{Fr}_i < 1.4$ produce no more than a shallow penetration ($k < 1$, figure 8). Accordingly, the only contribution to E_i is from the entrainment flux $E_{i,top}$ into the interfacial dome atop the incident jet, i.e. $E_i = E_{i,top} \propto \mathrm{Fr}_i^2$, as indicated in the region to the left of the first vertical line in figure 10.

Highly energetic impingements produce a deep penetration ($k > 1$). The lateral entrainment flux $E_{i,lat}$ into the counterflow of the penetrating fountain is relatively large compared with the fountain top entrainment flux $E_{i,top}$, i.e. $E_{i,lat} \gg E_{i,top}$. As $E_{i,lat} = E_{i,top}$ at $\mathrm{Fr}_i = 3.8$ (figure 10), the large-Fr_i regime occurs for $\mathrm{Fr}_i > 3.8$ (region to the right of the second vertical line).

Moderately energetic impingements, realised for $1.4 \leqslant \mathrm{Fr}_i \leqslant 3.8$ (the interval bounded by the two vertical lines), give rise to an intermediate regime in which the dominance of fountain top entrainment wanes with increasing Fr_i as lateral entrainment plays an increasingly active role.

A result that may not have been anticipated *a priori* is revealed upon plotting $E_{i,top}/E_i$ and $E_{i,lat}/E_i$ against Fr_i (figure 11). As $\mathrm{Fr}_i \to \infty$, the entrainment flux ratios asymptote to the constant values

$$\frac{E_{i,top}}{E_i} \approx 0.2 \quad \text{and} \quad \frac{E_{i,lat}}{E_i} \approx 0.8, \tag{6.2a,b}$$

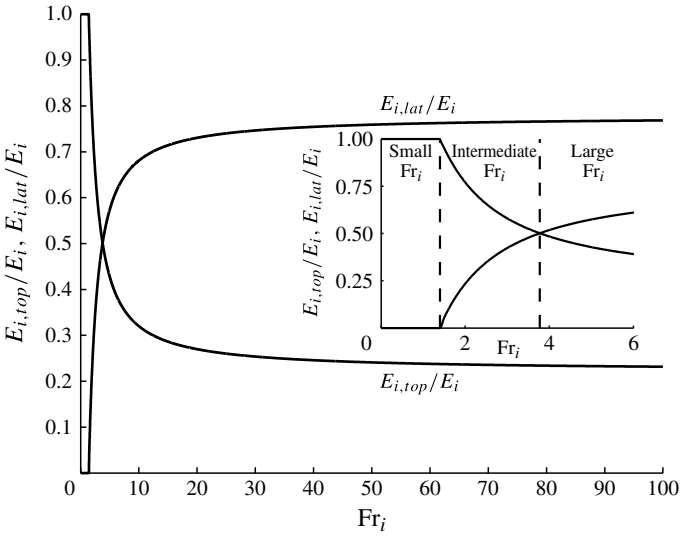

FIGURE 11. Entrainment flux ratios, $E_{i,top}/E_i$ and $E_{i,lat}/E_i$, as a function of Fr_i. The inset shows the same plot for $0 < \mathrm{Fr}_i \leqslant 6$ to highlight the three entrainment regimes.

i.e. in the high-Fr_i limit, approximately 20 % of the entrainment is via the fountain top and 80 % laterally. In this limit, one may regard the penetrating fountain as being globally 'self-similar', or exhibiting self-preserving behaviour, with respect to Fr_i. The inset of figure 11 shows a magnified view of the same plot to illustrate that $E_{i,top}/E_i$ and $E_{i,lat}/E_i$ vary rapidly for intermediate values of Fr_i, before gradually approaching their constant values at large Fr_i.

7. Comparison of predictions with existing experimental data

Figure 12(*a*) plots our theoretical solution for $E_i(\mathrm{Fr}_i)$ together with the existing experimental data from figure 1. Evidently, the predictions of our impingement dome model show very good agreement with the extensive data set of Kumagai (1984), thus affirming our theoretical result for small Fr_i (< 1.4), namely that E_i scales on the square of Fr_i. Furthermore, our predictions support the argument of Cardoso & Woods (1993) that Kumagai's data follows a power law of the form $E_i \propto \mathrm{Fr}_i^2$ for $\mathrm{Fr}_i \lesssim 1$. In contrast to Kumagai's empirical model (1.2), our solution indicates that E_i does not asymptote to a constant value for $\mathrm{Fr}_i \gg 1$, but rather scales linearly on Fr_i, following $E_i = 0.42\mathrm{Fr}_i$ for $\mathrm{Fr}_i > 3.8$ (figure 12*b*). Notably, Kumagai (1984) and Lin & Linden (2005) deduced their large-Fr_i constant-E_i result from a somewhat limited number of data points that span a relatively narrow range of Fr_i ($1 \lesssim \mathrm{Fr}_i \lesssim 3$). Arguably, the general trend for $\mathrm{Fr}_i \gg 1$ is better represented by the comprehensive data set of Baines *et al.* (1993) spanning $0.3 \lesssim \mathrm{Fr}_i \lesssim 26$. The predictions of our fountain model show good agreement with this data (figure 12*a*), thus affirming our theoretical result for large Fr_i, namely that E_i scales linearly on Fr_i. As anticipated based on our assumptions (§ 5), the fountain model marginally underpredicts E_i.

In the experiments of Baines *et al.* (1993), bulk vertical motions were imposed on the environment. For small Fr_i, the vertical velocity of the fountain at the interface was comparable with the velocity in the environment. As a consequence, the imposed flow in the environment is likely to have influenced E_i in the small-Fr_i regime. By

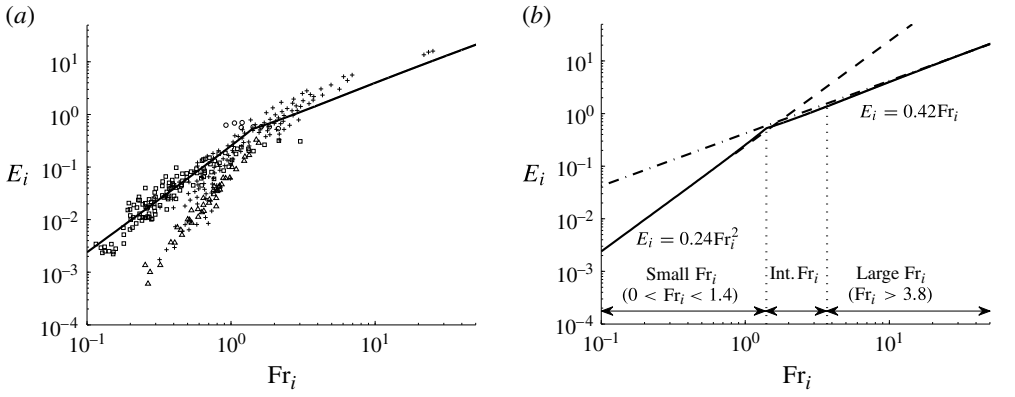

FIGURE 12. (*a*) Plot of E_i as a function of Fr_i: comparison of our theoretical solution (solid line) with the experimental data from figure 1. Symbols as in figure 1. (*b*) Power-law approximations to the full solution (solid line): dashed line is the power law $E_i = 0.24\mathrm{Fr}_i^2$ (3.26) and the dashed-dotted line is the best fit curve $E_i = 0.42\mathrm{Fr}_i$ to our fountain model for $\mathrm{Fr}_i > 3.8$. Dotted lines indicate the regime boundaries.

contrast, the environment we consider has no such motion imposed; this difference possibly explains why our predictions disagree with the data of Baines *et al.* (1993) for small Fr_i. Kumagai's experiments were performed in the absence of imposed vertical motions in the environment and our predictions agree well with his data.

In essence, vorticity drives interfacial entrainment and the power law that governs this process is determined by whether the vorticity is generated predominantly by baroclinic torque or by vertical shear. Plotting the power law approximations and the full solution for E_i in figure 12(*b*), we conclude that: (*a*) the quadratic power law $E_i = 0.24\mathrm{Fr}_i^2$ governs localised entrainment driven by baroclinic vortices around the periphery of an interfacial dome and (*b*) the linear power law $E_i = 0.42\mathrm{Fr}_i$ governs penetrative entrainment driven by shear-induced engulfment into a fountain.

8. Conclusions

The law governing the rate of turbulent entrainment across a stable density interface has been at the centre of a fascinating debate. Revisiting this fundamental problem, we examined theoretically the flow in an unconfined environment that is induced, and maintained, by the localised impingement of a steady turbulent jet on an interface separating two quiescent homogeneous fluid masses. Practical complexities associated with the inherent time-dependent coupling between the resulting entrainment flux across the interface and the development of a stratified intermediate layer were overcome by examining the large-time asymptotic state of the unconfined flow. This enabled us to deduce the dependence of the dimensionless entrainment flux E_i across the interface on the interfacial Froude number Fr_i.

For small-Fr_i flows ($\mathrm{Fr}_i < 1.4$), characterised by a semi-ellipsoidal interfacial dome atop the impinging jet, the entrainment flux is governed by a quadratic power law $E_i \propto \mathrm{Fr}_i^2$. For large-$\mathrm{Fr}_i$ flows ($\mathrm{Fr}_i > 3.8$), characterised by a fully penetrating turbulent fountain, the entrainment flux is governed by a linear power law $E_i \propto \mathrm{Fr}_i$. The solutions obtained (1.3) are in very good agreement with existing experimental data, thus lending support to the application of our models in engineering, the atmospheric sciences and oceanography.

Our work offers a simple framework for analysing, by means of tractable mathematical models, the complex problem of turbulent entrainment across an interface due to the localised impingement of a shear flow (e.g. jet, plume or fountain). Undeniably, the representation of turbulence, necessary to close the problem mathematically, sits at the heart of this framework. Mechanistic arguments based on small-Fr_i jet–interface interaction revealed that the essentials of turbulent entrainment in this regime are captured by a constant entrainment coefficient α (a ratio of the inflow velocity into the interfacial dome at a given height to the local vertical velocity near the dome perimeter). Whilst this parameterisation is consistent with the widely applied entrainment closure model of Morton *et al.* (1956), the question of what is the most appropriate value of α remains open. Given that our aim was a pragmatic one of determining the dependence of E_i on Fr_i, it is heartening that the exponent n in our entrainment law $E_i \propto \mathrm{Fr}_i^n$ is independent of α. Notably, n is also not influenced by the velocity profile adopted for the impinging jet. From experimental and practical viewpoints, it is encouraging, whilst perhaps fortuitous, that E_i is only weakly sensitive to α and that good agreement between our model and existing data is achieved with the commonly adopted value of $\alpha = 0.1$. Arguably, more sophisticated closure models may provide further insight into the entrainment process.

The dynamics have been classified into three regimes (small, intermediate and large Fr_i). The predicted sharp transition in E_i between the small-Fr_i and intermediate-Fr_i regimes is not anticipated in practice. To capture the dynamics of this transition, a model of the evolution from an interfacial dome to a penetrating fountain is required. Whilst the values of Fr_i that we have established as the regime boundaries depend on the entrainment coefficients chosen, our classification may provide an informative starting point for future experimental and numerical work. Finally, when the two-layer system considered is confined to a box or visual tank, interfacial entrainment may be influenced by secondary flows in the environment. This is currently under investigation.

Appendix A. Energy flux dissipated at the interface

A steady self-similar turbulent axisymmetric jet, of density ρ_1, with top-hat velocity profiles impinging on a density interface ($z = 0$) supplies mean kinetic energy flux $\mathscr{E}_i = \pi\rho_1 b_i^2 w_i^3/2$. Following Cardoso & Woods (1993), if a constant fraction $\mathscr{F}$ of $\mathscr{E}_i$ is dissipated, the flux of energy remaining is $(1-\mathscr{F})\mathscr{E}_i$. On physical grounds, the magnitude of the energy flux available for interfacial entrainment must be independent of the velocity profile adopted for the jet. Thus, the top-hat and Gaussian energy fluxes available after dissipation must be equal in magnitude, i.e.

$$(1-\mathscr{F})\,\frac{\pi}{2} b_i^2 w_i^3 = (1-\mathscr{F}_G)\,\frac{\pi}{6} b_{i,G}^2 w_{i,G}^3, \tag{A 1}$$

where the right-hand side is the energy flux supplied by a jet with Gaussian profiles and $\mathscr{F}_G = 0.5$ (Cardoso & Woods 1993). Equating the top-hat and Gaussian fluxes of volume and momentum yields $b_i = \sqrt{2} b_{i,G}$ and $w_i = w_{i,G}/2$. Substituting these expressions into (A 1) gives $\mathscr{F} = 1/3$.

It is instructive to examine the sensitivity of the entrainment flux E_i to changes in $\mathscr{F}$. We recall (§ 3.4) that $\mathscr{F}$ only influences the scaling factor A in our entrainment law $E_i = A\mathrm{Fr}_i^n$. Given that $C \approx 0.16$ (3.13) and $B \approx (1-\mathscr{F})/0.708$ (3.20), from (3.26)

$$A \sim 0.226(1-\mathscr{F})\sqrt{1.41(1-\mathscr{F})+1.5}. \tag{A 2}$$

Cardoso & Woods (1993) found that $0.4 \leqslant \mathscr{F}_G \leqslant 0.6$, which corresponds to $0.2 \lesssim \mathscr{F} \lesssim 0.47$. Thus, a 10 % change in $\mathscr{F}_G = 0.5$ results in A varying in the range $0.18 \lesssim A \lesssim 0.29$ (A 2). These values of A still agree well with the range of values reported by Zilitinkevich (1991) ($0.1 \lesssim A \lesssim 0.3$) and Kumagai (1984) ($0.1 \lesssim A \lesssim 0.25$). Hence, E_i is not highly sensitive to changes in $\mathscr{F}$.

REFERENCES

ANSONG, J. K., KYBA, P. K. & SUTHERLAND, B. R. 2008 Fountains impinging on a density interface. *J. Fluid Mech.* **595**, 115–139.

BAINES, W. D. 1975 Entrainment by a plume or jet at a density interface. *J. Fluid Mech.* **68** (2), 309–320.

BAINES, W. D., CORRIVEAU, A. F. & REEDMAN, T. J. 1993 Turbulent fountains in a closed chamber. *J. Fluid Mech.* **255**, 621–646.

BATCHELOR, G. K. 1967 *An Introduction to Fluid Dynamics*. Cambridge University Press.

BLOOMFIELD, L. J. & KERR, R. C. 2000 A theoretical model of a turbulent fountain. *J. Fluid Mech.* **424**, 197–216.

CARDOSO, S. S. S. & WOODS, A. W. 1993 Mixing by a turbulent plume in a confined stratified region. *J. Fluid Mech.* **250**, 277–305.

CHING, C. Y., FERNANDO, H. J. S. & NOH, Y. 1993 Interaction of a negatively buoyant line plume with a density interface. *Dyn. Atmos. Oceans* **19**, 367–388.

COFFEY, C. J. & HUNT, G. R. 2010 The unidirectional emptying box. *J. Fluid Mech.* **660**, 456–474.

COTEL, A. J. & BREIDENTHAL, R. E. 1997 A model of stratified entrainment using vortex persistence. *Appl. Sci. Res.* **57**, 349–366.

COTEL, A. J., GJESTVANG, J. A., RAMKHELAWAN, N. N. & BREIDENTHAL, R. E. 1997 Laboratory experiments of a jet impinging on a stratified interface. *Exp. Fluids* **23**, 155–160.

COTEL, A. J. & KUDO, Y. 2008 Impingement of buoyancy-driven flows at a stratified interface. *Exp. Fluids* **45**, 131–139.

FERNANDO, H. J. S. 1991 Turbulent mixing in stratified fluids. *Annu. Rev. Fluid Mech.* **23**, 455–493.

FERNANDO, H. J. S. & LONG, R. R. 1983 The growth of a grid-generated turbulent mixed layer in a two-fluid system. *J. Fluid Mech.* **133**, 377–395.

FISCHER, H. B., LIST, E. J., KOH, R. C. Y., IMBERGER, J. & BROOKS, N. H. 1979 *Mixing in Inland and Coastal Waters*. Academic Press.

HUNT, G. R. & COFFEY, C. J. 2010 Emptying boxes – classifying transient natural ventilation flows. *J. Fluid Mech.* **646**, 137–168.

KAYE, N. B., FLYNN, M. R., COOK, M. J. & JI, Y. 2010 The role of diffusion on the interface thickness in a ventilated filling box. *J. Fluid Mech.* **652**, 195–205.

KAYE, N. B. & HUNT, G. R. 2006 Weak fountains. *J. Fluid Mech.* **558**, 319–328.

KUMAGAI, M. 1984 Turbulent buoyant convection from a source in a confined two-layered region. *J. Fluid Mech.* **147**, 105–131.

LIN, Y. J. P. & LINDEN, P. F. 2005 The entrainment due to a turbulent fountain at a density interface. *J. Fluid Mech.* **542**, 25–52.

LINDEN, P. F. 1973 The interaction of a vortex ring with a sharp density interface: a model for turbulent entrainment. *J. Fluid Mech.* **60** (3), 467–480.

LINDEN, P. F. 1975 The deepening of a mixed layer in a stratified fluid. *J. Fluid Mech.* **71** (2), 385–405.

MCDOUGALL, T. J. 1978 Some aspects of geophysical turbulence. PhD thesis, University of Cambridge.

MIZUSHINA, T., OGINO, F., TAKEUCHI, H. & IKAWA, H. 1982 An experimental study of vertical turbulent jet with negative buoyancy. *Wärme-und Stoffübertragung.* **16**, 15–21.

MORTON, B. R., TAYLOR, G. & TURNER, J. S. 1956 Turbulent gravitational convection from maintained and instantaneous sources. *Proc. R. Soc. Lond.* A **234**, 1–23.

ROUSE, H. & DODU, J. 1955 Turbulent diffusion across a density discontinuity. *La Houille Blanche* **10**, 522–532.

SHAPIRO, M. A. 1980 Turbulent mixing within tropopause folds as a mechanism for the exchange of chemical constituents between the stratosphere and troposphere. *J. Atmos. Sci.* **37**, 994–1004.

SHY, S. S. 1995 Mixing dynamics of jet interaction with a sharp density interface. *Exp. Therm. Fluid Sci.* **10**, 355–369.

TURNER, J. S. 1966 Jets and plumes with negative or reversing buoyancy. *J. Fluid Mech.* **26** (4), 779–792.

TURNER, J. S. 1968 The influence of molecular diffusivity on turbulent entrainment across a density interface. *J. Fluid Mech.* **33** (4), 639–656.

TURNER, J. S. 1986 Turbulent entrainment: the development of the entrainment assumption, and its application to geophysical flows. *J. Fluid Mech.* **173**, 431–471.

WILLIAMSON, N., ARMFIELD, S. W. & LIN, W. 2011 Forced turbulent fountain flow behaviour. *J. Fluid Mech.* **671**, 535–558.

ZHANG, Y., BELLINGHAM, J. G., GODIN, M. A. & RYAN, J. P. 2012 Using an autonomous underwater vehicle to track the thermocline based on peak-gradient detection. *IEEE J. Ocean. Eng.* **37** (3), 544–553.

ZILITINKEVICH, S. S. 1991 *Turbulent Penetrative Convection*. Avebury Technical.